HAL
archives-ouvertes.fr

EIS study of iron and steel corrosion in aqueous solutions at various concentrations of dissolved H2S : impact of oxygen contamination.

Martien Duvall Deffo Ayagou, Christophe Mendibide, Claude Duret-Thual, Jean Kittel, Nicolas Ferrando, Eliane Sutter, Thi Tuyet Mai Tran, Bernard Tribollet

▶ To cite this version:

HAL Id: hal-02462542

https://hal-ifp.archives-ouvertes.fr/hal-02462542

Submitted on 31 Jan 2020

EIS STUDY OF IRON AND STEEL CORROSION IN AQUEOUS SOLUTIONS AT VARIOUS CONCENTRATIONS OF DISSOLVED H₂S: IMPACT OF OXYGEN CONTAMINATION.

Martien Duvall Deffo Ayagou, Christophe Mendibide, Claude Duret-Thual
Institut de la Corrosion – Site de Saint-Etienne
Zone d'activités du Parc secteur Gampille
42490 Fraisses, France

Jean. Kittel
IFP Energies nouvelles
Rond-Point de l'échangeur de Solaize
BP3, 69360 Solaize, France
Jean.kittel@ifpen.fr

Nicolas Ferrando
IFP Energies nouvelles
1 et 4 avenue de Bois-Préau
92852 Rueil-Malmaison, France

Eliane Sutter, Thi Tuyet Mai Tran,
Bernard Tribollet
Laboratoire Interfaces et Systèmes
Electrochimiques (LISE), UMR 8235 CNRS-UPMC
75252 Paris Cedex 05, France

ABSTRACT

Mildly acidic water containing dissolved H_2S presents a strong risk in the cracking of low-carbon steels. Several studies on H_2S cracking mechanisms have shown that the main driving force is linked to the ability of H_2S to promote hydrogen entry into the bulk material. Standard test methods have been developed and published as NACE technical standards (e.g. NACE TM0284 and NACE TM0177) to aid materials selection in the oil and gas sector. Though it is recognized that oxygen pollution should be avoided during H_2S cracking tests, there is a lack of experimental data to illustrate the effects of a small oxygen pollution. Dissolved oxygen concentrations greater than the recommended upper limit (50 parts per billion) can easily be obtained in the case of poor laboratory practices.

This paper will focus on the interactions between oxygen and H_2S on electrochemical behavior of unalloyed steel. A continuous O_2 injection at a level corresponding to 500 ppb is applied, together with H_2S bubbling in our test solutions, for periods lasting the same order as SSC standard tests. Steel surface reaction phenomena/corrosion rates in H_2S saturated solution, with or without oxygen pollution, are studied using electrochemical impedance spectroscopy.

The evolution of corrosion rates obtained from impedance analysis was compared to two other independent methods: i/ weight loss measurements and, ii/ hydrogen permeation. Without O_2 pollution, a permeation efficiency of 100% was obtained, as expected. Permeation current density was thus found to match precisely with the corrosion current density determined by impedance analysis at different times. On the other hand, when a continuous O_2 pollution was added in the system, significantly higher corrosion rates were observed, associated with test solution acidification. At the same time, permeation efficiency was decreased by up to one order of magnitude.

Key words: H_2S, O_2, HIC, SSC, hydrogen permeation, hydrogen embrittlement, X65 steel.

INTRODUCTION

Materials used in oil and gas industries are exposed to H_2S-containing (sour) environments, which is corrosive and known to promote hydrogen entry into steels. This may lead to several types of failures such as hydrogen-induced cracking (HIC), sulfide stress cracking (SSC), or stress-oriented hydrogen induced cracking (SOHIC). The corrosion and hydrogen embrittlement of steels in H_2S containing environments has been studied for several decades. Standard test methods have been developed for the selection and the qualification of steels for use in H_2S containing environments, such as NACE[a] TM0177 and TM0284.[1; 2] These standards strongly recommend the exclusion of oxygen entry in test environments. For instance, it is stated that *"obtaining and maintaining an environment with minimum dissolved O_2 contamination is considered very important"*. It is also mentioned that, "O_2 contamination may induce an increase of the corrosion rate and reduce hydrogen evolution and hydrogen entry into the steel", although *"systematic studies of the parameters affecting these phenomena have not been reported in the literature"*.

Oxygen pollution of a testing medium can be brought about in a number of ways, including; an incorrect or insufficient deaeration of the initial test solution; a poor sealing of test reactors; the use of plastic tubing permeable to oxygen; and a multitude of operations during the test (solution sampling, pH adjustment, etc.). In the present study, the impact of a continuous ingress of gaseous O_2 in a test solution, during a corrosion test with aqueous H_2S, is investigated. Song et *al.*[3] have reported that a solution bubbled with a mixture of H_2S and O_2 continuously acidifies and does not rise back to neutrality even after purging out H_2S with an inert gas (argon, nitrogen). Such an experimental finding is in good agreement with the reaction pathway proposed by Crolet and Pourbaix*,*[4] showing that O_2 and H_2S can react to form dissolved thiosulfate or tetrathionate ions. In both cases, H^+ ions are also produced, resulting in the measured decrease in pH. The produced S-O compounds could, then, modify the kinetics of hydrogen entry and surface corrosion mechanisms. For instance, Kuo et *al.*, have shown that the presence of thiosulfate in chlorinated H_2S medium significantly increases the corrosion rate of immersed steels.[5] These authors used anodic polarization experiments and microscopic observations of the corroded surface to conclude that thiosulfate ions participate in electrochemical-redox corrosion reactions. It is well-discussed that H_2S promotes hydrogen entry in steels via sulfur adsorbates.[6–8] Metal surface reactions with O_2 or with $O_2 – H_2S$ reaction products may influence the hydrogen entry process. Indeed, some authors propose using thiosulfate solutions to replace H_2S in cracking experiments.[9; 10] Indeed, they suggest that thiosulfate reduction at the metal surface could result in the formation of H_2S, that may increase hydrogen permeation through the material.

In summary, oxygen traces in H_2S containing environment could modify the system in three distinct ways, i.e. by:

- changing the composition of the corrosive environment;
- modifying the corrosion rate and the nature of corrosion deposits;
- interacting with H_2S adsorbates and changing the efficiency of hydrogen entry.

In this article, pure iron, in the annealed condition, and a sour-service grade X65 are exposed to H_2S saturated test solutions. Two types of solutions were compared: 35 g/L NaCl or NACE A consisting of 5.0 wt% NaCl and 0.5 wt% glacial acetic acid in deionized water. A gas supply system that permits a well-controlled O_2 entry in the test cell is used, at a partial pressure of 1 – 1.5 kPa, thus corresponding to 500 ppbw (parts per billion by weight) dissolved O_2 at equilibrium. Both corrosion and hydrogen uptake tests are conducted using a classic two-chamber hydrogen permeation cell. At the entry side, electrochemical impedance spectroscopy (EIS) is used to evaluate the corrosion behavior of the iron membrane in the H_2S medium. At the exit side, hydrogen permeation is measured by anodic extraction. Chemical analysis of the test solution identifies the reaction products of O_2 and H_2S.

---

[a] NACE International, 1440 South Creek Dr, Houston Texas 77084-4906

EXPERIMENTAL PROCEDURE

Details of the entire experimental methodology are provided in previous publications[11; 12]. Here, we provide only a summary of the main methods.

Control of O_2 contamination in the test media

Two types of tests were carried out in this study, i.e. those with and without O_2 contamination. Reference conditions without O_2 contamination correspond to dissolved O_2 level below 10 ppbw. During preliminary calibration tests, CO_2 was used in place of H_2S in order to avoid $H_2S + O_2$ reactions. When O_2 contamination was considered, it was introduced in a continuous manner into the test cell through an independent gas supply line. Each gas line was equipped with a mass flow controller (MFC), allowing the control of H_2S and O_2 partial pressures in the gas stream bubbling in the test solution throughout the experiment. In this paper, P_{O2} was set to 1.3 kPa (13 mbar), corresponding to 500 ppbw in solution saturation. Since the recent revisions of NACE TM0177 and NACE TM0284 express O_2 limits in units of ppbw, this unit is used in the paper. Though it is stated that the parameter controlled was, indeed, O_2 partial pressure.

Materials and corrosive medium

The main part of the study was carried out in a model system (with pure Fe), whose characteristics were selected with the aim of being as simple as possible and avoid material-related complications. To be clear, the pure Fe (99.5 % purity) was heat treated under vacuum at 900 °C for 30 minutes in order to normalize the microstructure and reduce fabrication artefacts (high dislocation density, residual stress, irregular microstructure etc.) that interfere with the through-material diffusion of hydrogen. Test solutions consisted of 35 g/L NaCl without acids or buffering species. H_2S at various partial pressures between 0.1 MPa and 0.1 kPa were used (for P_{H2S} below atmospheric pressure, gas cylinders containing a mixture of H_2S and N_2 were used).

In addition, comparative tests were conducted in a system more representative of oil and gas production. Pure iron was replaced by X65 linepipe steel, whose composition is given in Table 1. A test solution representative of SSC qualification tests (NACE TM0177) was used. It was composed of 5 % NaCl and 0.5 % acetic acid (NACE A solution) with H_2S partial pressure of 0.1 MPa. For both systems, comparative tests with and without continuous O_2 contamination at 500 ppbw were performed.

Table 1
Chemical composition of API 5L X65 (% weight)

Element	Al	Cr	Cu	Mn	Ni	Si	Ti+Nb+V	C	P	S	Fe
API[b] 5L X65	0.03	-	-	1.39	-	0.31	0.062	0.044	0.012	<0.001	Bal

Corrosion and hydrogen permeation test cells

Exposure of iron and steel specimens was carried out in a jacketed Devanathan-Stachurski type cell.[13] The experimental setup was made of twin cells separated by the iron/steel membrane. The solution

---

[b] American Petroleum Institute (API) , 1220 LSt, N.W., Washington, DC 20005-4070

temperature was maintained at 24 +/- 2°C, through circulating thermally-controlled water through the cell's jackets. The iron/steel membrane was used for two distinct types of electrochemical measurements, carried out simultaneously. EIS measurements were performed at the charging side left at the free corrosion potential (E_{corr}). At the same time, the exit surface of the membrane covered with a Pd deposit was held in a deoxygenated 0.1 mol.L^{-1} NaOH solution and polarized at an anodic potential of 250 mV vs. Hg/HgO (1M KOH) providing a direct measurement of the hydrogen flux across the steel membrane. Membrane thickness was 0.5 x 10^{-3} m, and the exposed area was 16 x 10^{-4} m² on both sides.

In addition to the permeation membrane, weight-loss specimens of the same material as the permeation membrane (0.009 m x 0.009 m x 0.0005 m) were also introduced into the charging cell. These coupons were used for weight-loss corrosion rate evaluation, as well as surface analysis by Scanning Electronic Microscopy (SEM), and X-Ray Diffraction (XRD). Accounting for the surface areas of the permeation membrane and iron coupons, the ratio between test solution volume and exposed surface was close to 20 mL/cm². No stirring was applied except that provided by gas bubbling though frit glass.

TESTS IN MODEL SYSTEMS AT VARIOUS H$_2$S CONCENTRATION

In order to determine the impact of O$_2$ contamination on the sour test solution, several tests were conducted with pure iron exposed to 35 g/L NaCl solution at various H$_2$S partial pressures between 0.1 MPa and 0.1 kPa. Several types of measurements were carried out: 1) continuous in-situ pH measurement and periodic sampling of test solution for chemical analysis; 2) weight-loss and surface analysis of small coupons; 3) EIS at the entry face of the membrane; 4) hydrogen permeation at the exit face of the membrane.

Figure 1 shows the evolution with time of test solution pH with or without oxygen.
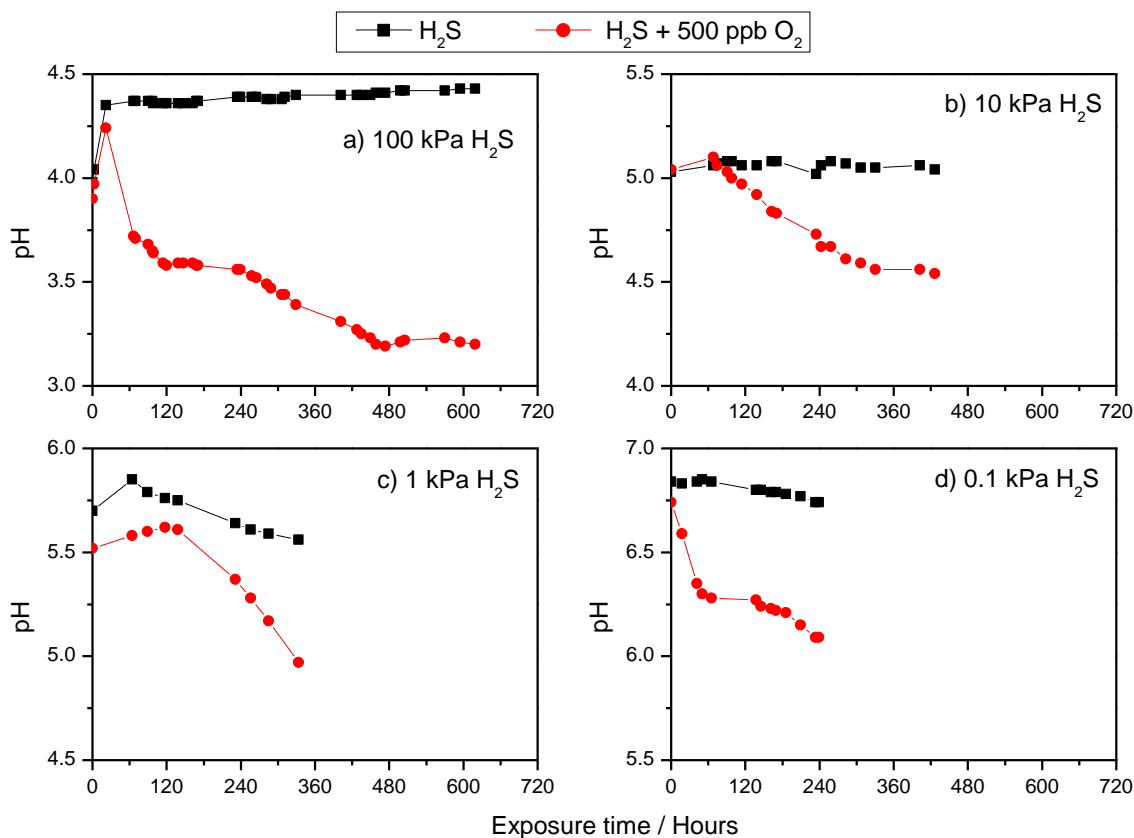

Figure 1: Time evolution of pH of test solutions at various H$_2$S partial pressures of (a) 100 kPa (b) 10 kPa (c) 1 kPa and (d) 0.1 kPa. Impact of continuous O$_2$ contamination corresponding to 500 ppb weight (P$_{O2}$ = 1.3 kPa).

For short exposures times, no significant differences were measured between the test with O_2 contamination and the control test without O_2. Initial pH values (t = a few hours) were determined by acid gas content (i.e. P_{H2S}) and the FeS solubility equilibrium. Saturated pH values calculated with Cormed™[c] are reported in Table 2 and compared with experimental values at short exposures. With the exception of the lowest P_{H2S}, an excellent match is found between experimental and calculated values. As expected, the reference tests without O_2 contamination did not exhibit significant changes of pH with time, once the saturated value is attained. On the contrary, O_2 contamination systematically induces an acidification of test solution. The rate of pH drop is of the same order of magnitude for all P_{H2S} and lies between 0.15 and 0.3 pH unit per 100 hours exposure. Considering the usual duration of a standard SSC test (720 hours), we anticipate that a pH drop more than 1 pH unit is entirely possible.

Table 2
Comparison between experimental pH at the beginning of the tests and calculated pH at FeS saturation in 35 g/L NaCl solution at 24 °C.

	100 kPa	10 kPa	1 kPa	0.1 kPa
Experimental pH without O_2	4.3	5.0	5.7	6.8
Experimental pH with O_2	4.2	5.0	5.5	6.7
Calculated pH	4.3	5.0	5.6	6.3

In order to investigate such test solution acidification in the presence of O_2 contamination, periodic sampling of the test solution was conducted for the experiments at 100 kPa H_2S and 10 kPa H_2S. Analysis by ionic chromatography (IC) showed that sulfate (SO_4^{2-}) was the main species formed, as a result of dissolved O_2 – H_2S reactions. Its concentration increased linearly with time in presence of O_2 contamination, while it stayed at minute levels in reference conditions without O_2 (Figure 2). According to the literature, reaction paths leading to sulfate involve an intermediate step with thiosulfate ($S_2O_3^{2-}$) formation accompanied by the release of H^+:[14; 15]

$$2 \, H_2S + 2 \, O_2 \rightarrow S_2O_3^{2-} + H_2O + 2 \, H^+ \qquad \text{(Reaction 1)}$$
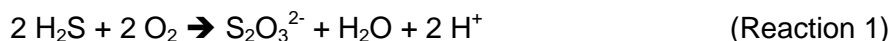
The more stable sulfate species may then be formed by various paths, e.g. by direct oxidation:

$$S_2O_3^{2-} + 1/2 \, O_2 \rightarrow SO_4^{2-} + S \qquad \text{(Reaction 2)}$$

Apart from direct oxidation, thiosulfate is known to enhance iron and steel corrosion, with additional intermediate reactions involving H_2S and elemental sulfur formation.[10; 16]

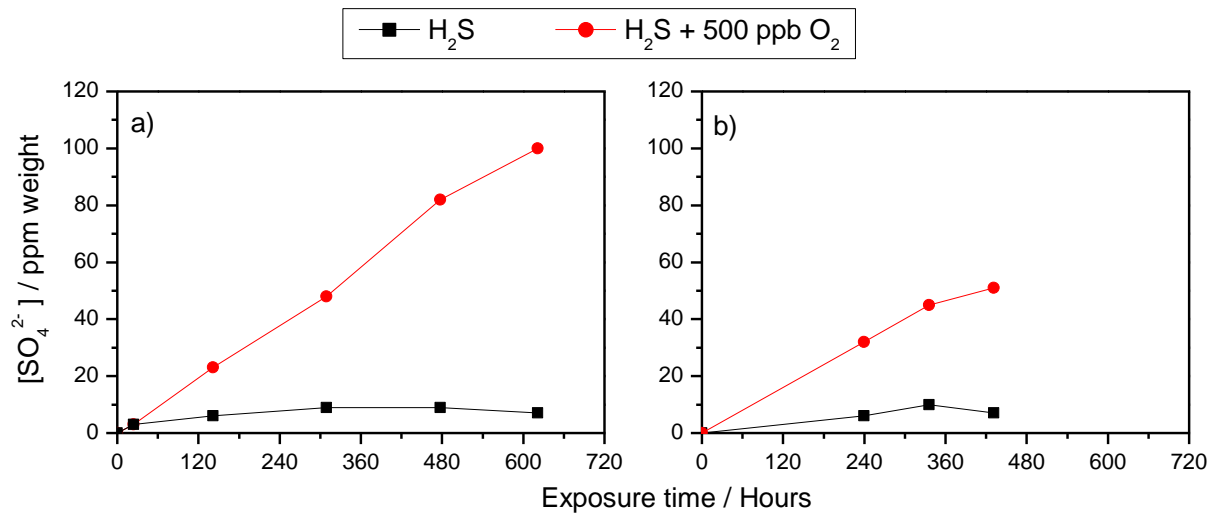[c] Corrosive Medium, calculation tool developed by Total, France

Figure 2: Time evolution of sulfate concentration for the tests at (a) 100 kPa and (b) 10 kPa H$_2$S in model systems.

Such sensitive measurements of sulfate concentrations in solution samples could indicate O$_2$ contamination during SSC qualification tests. Indeed, NACE TM0177 mentions that '*oxygen contamination is evident by a cloudy (opaque) appearance of the test solution when the H$_2$S gas enters the test vessel*'. However, no such cloudiness is noted during our tests, except for some preliminary experiments without steel coupons. As soon as steel is present, darkening of the test solution occurs with iron sulfide precipitation, masking any other color changes. Changes of pH in the acidic direction or chemical detection of sulfates might thus represent more robust indicators of oxygen contamination.

The corrosion rates of pure iron weight-loss coupons exposed to tests solutions at various P$_{H2S}$ and with or without O$_2$ contamination are compared in Table 3. Four replicates were performed under 100 kPa H$_2$S, from which standard deviations were determined. All other tests were conducted only once. As expected, corrosion rates in reference conditions without O$_2$ decrease monotonically as P$_{H2S}$ decreases. The corrosion rate drops from 0.5 mm/year for the test conducted with 100 kPa H$_2$S, to 0.1 mm/year at 0.1 kPa H$_2$S. This decrease of corrosion rate correlates well with the increase in bulk solution pH (with decreasing dissolved H$_2$S content).

In the presence of O$_2$ contamination, a systematic acceleration of corrosion is seen, relative to the control tests without O$_2$. In addition, the amplitude of this aggravation increases as P$_{H2S}$ decreases: while corrosion rate is doubled for the tests at 100 kPa and 10 kPa H$_2$S, it increases by more than one order of magnitude at the lowest H$_2$S concentrations. Surprisingly, highest corrosion rates are obtained with 1 kPa and 0.1 kPa H$_2$S with 500 ppb weight O$_2$ compared to the tests at 100 kPa and 10 kPa H$_2$S, in spite of lower pHs. The reasons are not fully understood at this stage, but are suspected to relate to a lower protectivity of the iron sulfide scale, a contribution of some H$_2$S-O$_2$ reaction chemistry, and indeed oxygen corrosion.

Table 3
Impact of O$_2$ contamination on corrosion rate of pure iron weight-loss coupons exposed to 35 g/L NaCl solution saturated with H$_2$S at various partial pressures for 2 to 4 weeks.

	100 kPa H$_2$S	10 kPa H$_2$S	1 kPa H$_2$S	0.1 kPa H$_2$S
H$_2$S	489 +/- 68 µm/year	284 µm/year	163 µm/year	101 µm/year
H$_2$S + 500 ppb O$_2$	976 +/- 248 µm/year	523 µm/year	2257 µm/year	1111 µm/year

In order to gather more information on corrosion mechanisms and their evolution as a function of time, periodic EIS measurements were conducted for the tests at 100 kPa and 10 kPa H_2S. While EIS spectra measured with or without O_2 contamination were similar at the beginning of the tests, significant differences present themselves at longer exposure times, typically after 2 to 3 days (Figure 3). One of our previous papers reports a detailed EIS characterization of pure iron exposed to 100 kPa H_2S , as being a two-step anodic reaction with an adsorbed intermediate.[12] The equivalent circuit corresponding to this mechanism is presented in Figure 4.a. The charge transfer resistance from which corrosion rate is calculated is represented by the diameter of the high frequency semi-circle observed in Nyquist plots (see Figure 3.a) measured after 2 hours or 47 hours. For longer exposure times typically above 160 hours, we discuss that the evolving porous and conductive iron sulfide film begins to considerably modify the shape of impedance diagrams, with a behavior typical of porous electrodes. Impedance diagrams flatten out and tend towards a single line at 45° in the Nyquist plots. A porous and conductive film contribution must then be introduced to the EIS equivalent circuit, as illustrated in Figure 4.b. This porous electrode behavior was not observed when O_2 contamination was present at 500 ppb weight, and all EIS spectra could be analyzed with the EC of Figure 4.a.[11] From an electrochemical point of view, it may suggest a lower and decreasing charge transfer resistance (higher corrosion rate) with time, in the presence of oxygen.
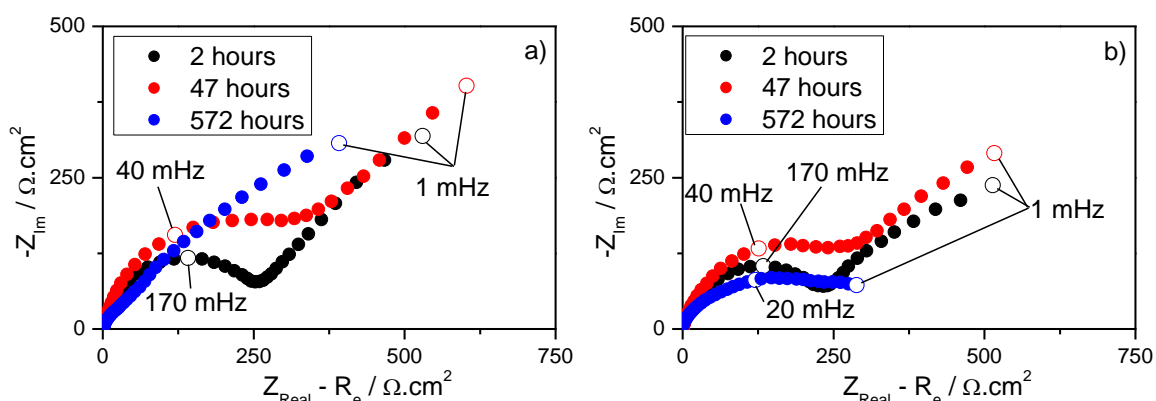

Figure 3: Typical impedance of pure iron in 35 g/L NaCl solution saturated with 100 kPa H_2S at various exposure times, without (a) and with (b) O_2 pollution.
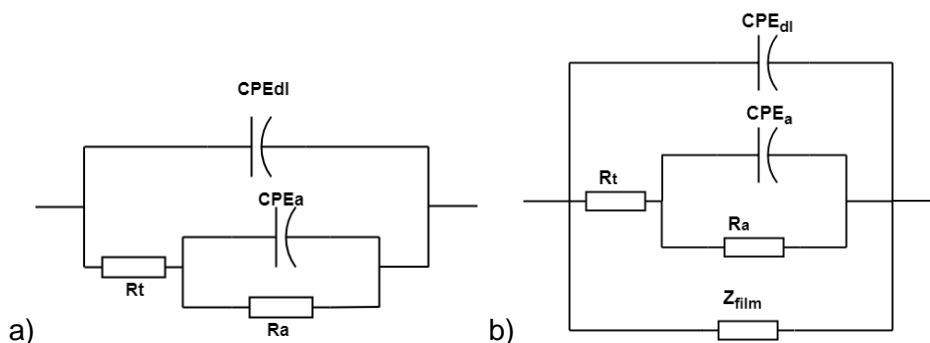

Figure 4: Equivalent circuits (EC) used for the analysis of EIS diagrams (a) at short immersion times and, (b) at longer immersion times when the conductive FeS film cannot be neglected anymore.

Time evolution of corrosion rates could then be calculated from R_t determined by EIS analysis, and the application of the Stern and Geary relationship and Faraday's law. Figure 5 presents the results obtained at 100 kPa and 10 kPa. They confirm that corrosion rate is enhanced in case of a continuous O_2 contamination. In addition, we note that the timing of the increase in corrosion rate over the sample exposure period correlates well with the accumulation of dissolved O_2 - H_2S reaction products and test solution pH drop.
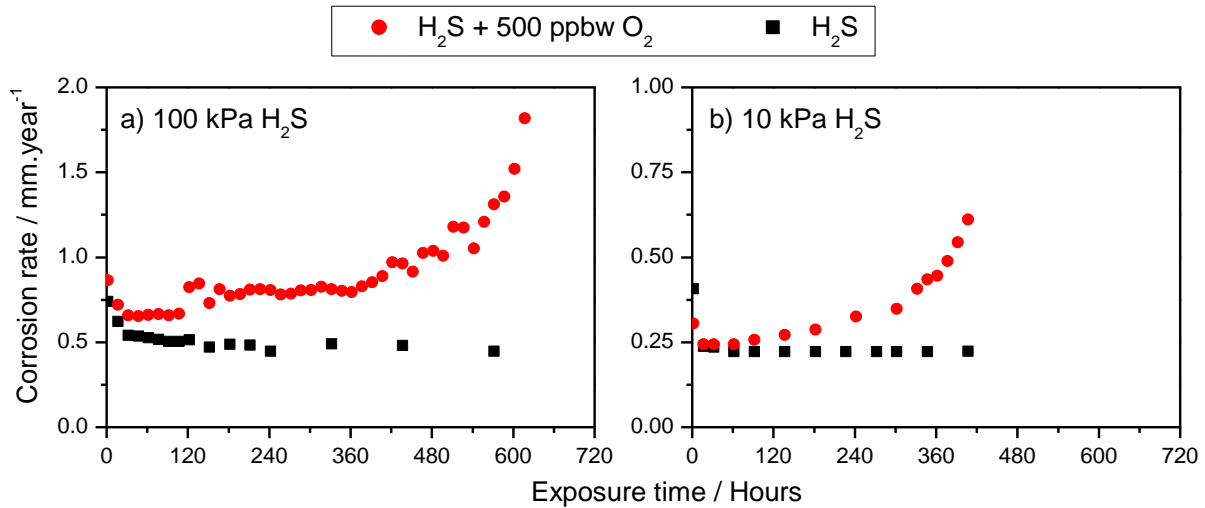
Figure 5: Time evolution of corrosion rates of pure iron determined from EIS analysis, for the tests at 100 kPa and 10 kPa H₂S.

As hydrogen permeation measurements (on the anodic extraction side) were conducted simultaneously with EIS (at the H-entry surface), it is interesting to compare the evolution of corrosion current density (J_{corr}, from R_t) with the hydrogen permeation current density (J_{perm}), through the determination of H-permeation efficiency (E_{perm}) as the quotient of J_{perm}/J_{corr}. A comparison of J_{perm} and E_{perm} is illustrated on Figure 6, where hydrogen permeation current densities are plotted with time, for the experiments exposed to 100 kPa and 10 kPa H₂S-media.

In acidic media containing H₂S, the proton reduction is indeed the main cathodic reaction, and one might thus expect a direct correlation with hydrogen permeation – as long as there is (i) no significant impediment to H-entry in the permeation sample (e.g. in the presence of H-entry promoters) (ii) that no significant H-trapping in the bulk material takes place (e.g. the use of a thin, high purity material) (iii) highly efficient H-measurement at the exit surface (e.g. with palladium deposition for anodic H-extraction) [7; 17]. Looking at Figure 6, we note that a permeation efficiency close to 100 % is obtained at 100 kPa when no O₂ contamination was present, and thus these criteria are met satisfactorily in the current study.
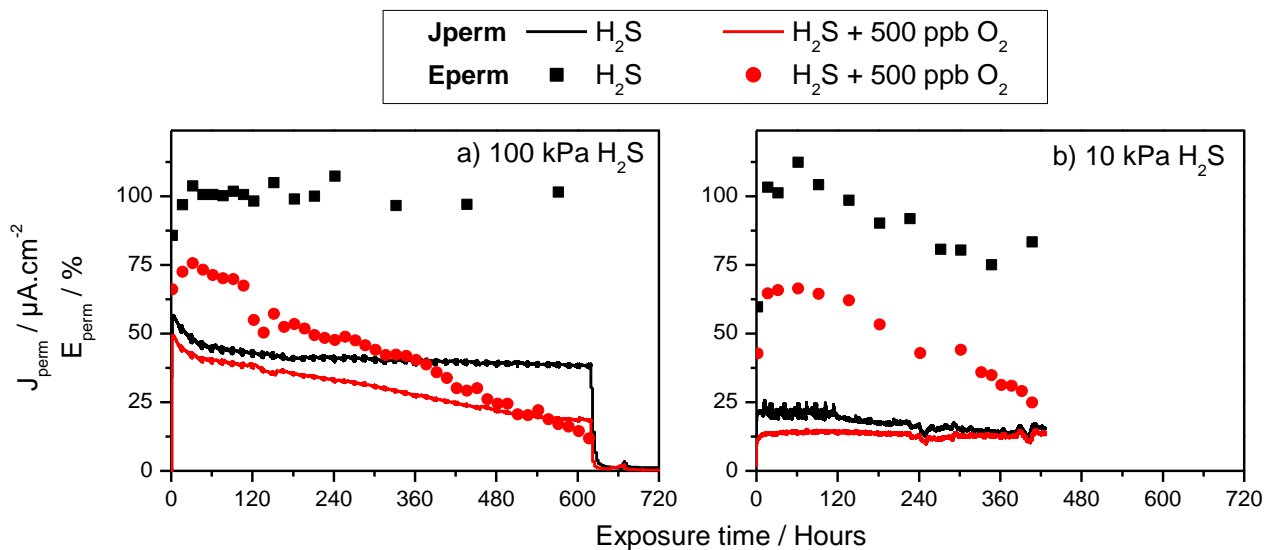

Figure 6: Time evolution of hydrogen permeation and permeation efficiency (E_{perm}) for the tests at 100 kPa and 10 kPa H₂S.

Conversely, with O_2 contamination (red plots of Figure 6), a decrease of hydrogen permeation current density is observed, together with a continuous drop of the permeation efficiency. Such phenomena could be explained by changes to the surface reaction rates of hydrogen uptake. The appearance of additional cathodic reactions involving H_2S – O_2 reaction products is also considered. Though not identified at this stage, we infer that such processes limit the entry of hydrogen into the metal.

TESTS ON X65 STEEL IN NACE A SOLUTION

In addition to the tests in model solutions, additional experiments were performed with an oilfield material alloy (API[d] X65), exposed to the model solution without buffer (35 g/L NaCl) or to NACE A solution. As a reminder, this solution is commonly used for testing SSC resistance of low alloy steels, and is composed of 5 % NaCl and 0.5 % acetic acid, saturated under 100 kPa H_2S. As for the tests in the model solution, the ratio between the NACE A test solution volume and the metal surface was maintained at 20 mL/cm². Compared to previous tests on pure Fe, a slightly lower P_{O2} was used (1 kPa), corresponding to 300 ppb weight at equilibrium. The evolution of pH during these tests are illustrated in Figure 7.
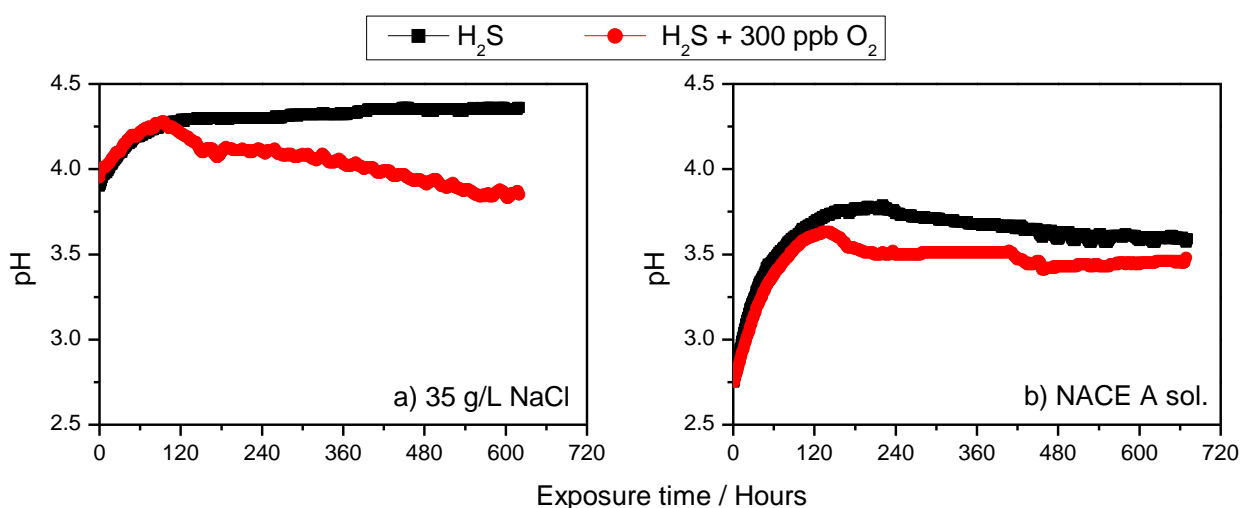

Figure 7: Time evolution of pH for various experiments with X65 membranes, exposed to 35 g/L or NACE A solution with 100 kPa H_2S. Impact of continuous O_2 contamination corresponding to 300 ppb weight (P_{O2} = 1 kPa).

In model solution (35 g/L NaCl, Figure 7.a) the same trend as already observed with pure iron membranes is reproduced. O_2 contamination results in a continuous acidification of the test solution. The rate of pH drop is slightly slower than previously observed on pure iron membranes, most likely due to the lower P_{O2} used with X65 membrane (300 ppb vs. 500 ppb). In NACE A solution, the impact of O_2 is less pronounced, although a weak acidification is noted. The lower initial pH and the buffering effect of acetates could explain the better stability of test solution pH. However, one must keep in mind that even if pH change is moderate, reaction products between O_2 and H_2S still accumulate, and may influence corrosion and hydrogen permeation. A comparison of corrosion rates for these tests is illustrated in Table 4. Similar to the model solution (35 g/L NaCl), O_2 contamination also accelerates pure Fe corrosion in NACE A solution by a factor of 2. Thus, the decrease in pH is not the only factor to

---

[d] American Petroleum Institute, Washington, DC (USA)

explain the rise of the corrosion rate in presence of O_2. In contrast, the X65 weight loss measurements depict a 50% relative increase in the model solution, and a consistent corrosion rate 'doubling' in the NACE A solution, both with O_2 pollution.

Table 4
Weight-loss corrosion rates of pure iron and X65 coupons for various tests in 35 g/L NaCl solution or NACE A solution.

	35 g/L NaCl		NACE A
	Pure iron	*X65*	*X65*
100 kPa H_2S	489 +/- 68 µm/year	508 µm/year	914 µm/year
100 kPa H2S + O_2*	976 +/- 248 µm/year	770 µm/year	1900 µm/year

* O_2 content was 500 ppbw for the test on pure iron, and 300 ppbw for the tests on X65 steel

EIS and hydrogen permeation measurements were equally carried out for the tests with X65 membrane. In 35 g/L NaCl solution, the results are markedly similar to those obtained with the pure iron membrane, i.e. an anodic impedance with a porous electrode behavior for long exposures in reference conditions without O_2, and a linear decrease of permeation rate for the test with O_2 contamination. Indeed, it shows that pure Fe can perform well as a model material for pipeline steels with complicated microstructures.

By contrast, the results in NACE A solution present several differences against those obtained in 35 g/L NaCl. Impedance diagrams in Figure 8 depict a single semi-circle, and no inclination at 45° for long exposures without O_2. Furthermore, the diameter of the high frequency semi-circle, believed to represent the charge transfer resistance, exhibits a continuous increase with exposure time; this feature remains at stable values in 35 g/L NaCl solution (without O_2). In presence of O_2 contamination, the evolution of R_t with time is similar to that already observed in 35 g/L NaCl, i.e. it reaches a maximum after 100 to 200 hours exposure, and then decreases with time.
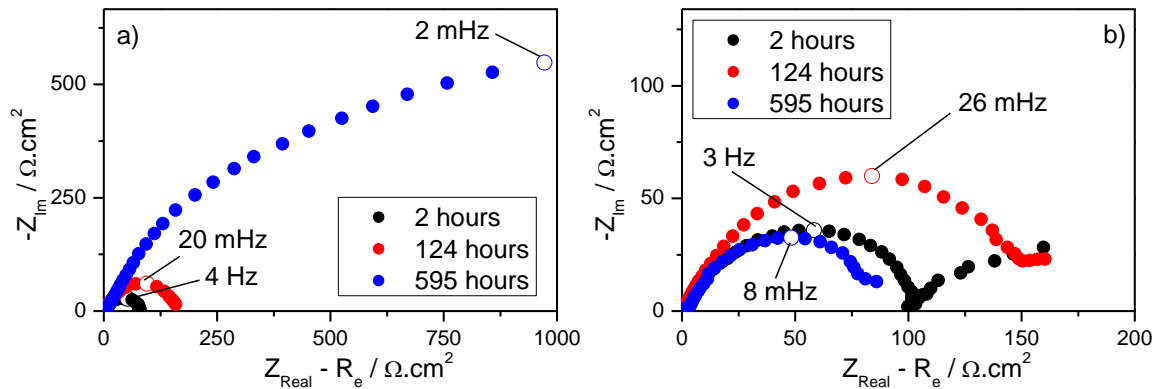

Figure 8: EIS diagrams of X65 membrane exposed to NACE A solution with 100 kPa H_2S at various exposure times, without (a) and with (b) O_2 pollution.

Time evolution of the corrosion current densities, determined from R_t values derived from EIS spectra, are plotted on Figure 9. Hydrogen permeation current densities, and permeation efficiencies (E_{perm}) are also plotted on the same graphs.

Without O_2 contamination (Figure 9.a), the permeation efficiency maintains 50 %, throughout the 4-week exposure period. We present two hypotheses to explain why E_{perm} is not 100 %, compared to observations for pure Fe in 35 g/L NaCl solution. i) The more complex microstructure of X65 steel compared to annealed pure iron might introduces hydrogen diffusion limitations; ii) an additional non-

hydrogenating cathodic reaction associated with acetic acid direct reduction, contributes to the corrosion current.[18] This test in NACE A solution without O_2 also presents another more significant and interesting difference with the model system: for long exposures, typically above 300 hours, a simultaneous decrease of the corrosion rate and of the permeation rate is observed, reaching values close to zero or a few µA/cm². We anticipate that this decrease is associated with the formation of a highly protective corrosion product layer, that was not observed on pure iron in 35 g/L NaCl solution.

With O_2 contamination (Figure 9.b), J_{corr} and E_{perm} follow similar evolutions than the ones observed with the model system, i.e. continuous increase of J_{corr} and decrease of E_{perm}. However, contrary to what was observed in the model system, the J_{perm} maintains a stable value after the initial decrease during the first days of immersion.
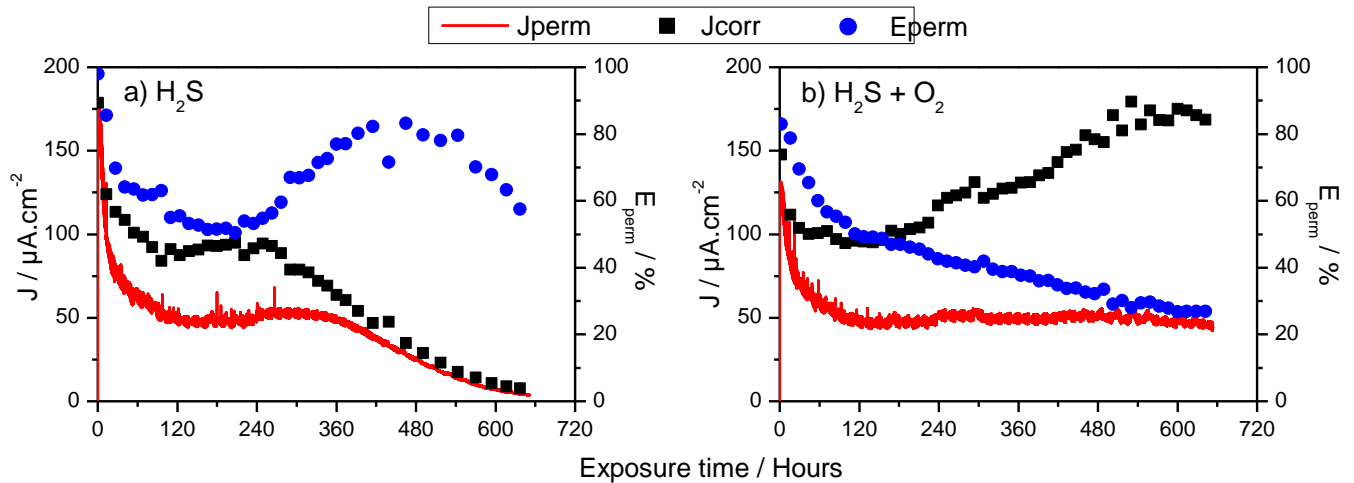

Figure 9 : Time evolution of corrosion current densities, hydrogen permeation current densities, and permeation efficiency (E_{perm}) for the tests on X65 in NACE A solution, without (a) and with (b) O_2 pollution.

CONCLUSIONS

The effect of traces of oxygen on the corrosion and hydrogen permeation across pure iron and API X65 low alloy steel was studied in a 35 g/L NaCl model solution and NACE A test solution, as a function of time over 3 to 4 weeks. H_2S concentrations ranging from 100 kPa to 0.1 kPa were used. O_2 pollution was introduced in a continuous manner in the test gas, at a partial pressure of 1 to 1.3 kPa corresponding to 300 to 500 ppb weight dissolved O_2 at equilibrium. The following conclusions are drawn from this study:

- O_2 pollution in an H_2S-saturated solution has strong influence on, and modifies the test solution chemistry. Sulfate was identified as the main stable soluble reaction product. $H_2S – O_2$ reactions also lead to test solution acidification. In a non-buffered model solution containing 35 g/L NaCl, the rate of acidification was comprised between - 0.15 and - 0.30 pH unit per 100 hours exposure. Acidification is less pronounced in NACE A solution due to a lower initial pH and to the buffering effect of acetates.
- As expected, O_2 pollution is found to increase significantly corrosion rates. The aggravation is more pronounced at the lowest P_{H2S} (one order of magnitude at 1 and 0.1 kPa H_2S, and a factor of 2 at 100 and 10 kPa).
- Simultaneous measurements of EIS and hydrogen permeation, respectively at the entry and exit faces of metal membranes, allowed for the determination of the time evolution of corrosion current density, hydrogen permeation current density, and of their ratio (E_{perm}). Without O_2

contamination, high permeation efficiencies were obtained both in 35 g/L NaCl and NACE A solutions at 100 kPa and 10 kPa H_2S. On the other hand, O_2 contamination systematically induced a continuous decrease of permeation efficiency.

- Another striking difference was observed when comparing long term behavior of materials in our model solution (35 g/L NaCl) and in NACE A solution, without O_2 contamination. In 35 g/L NaCl solution, both the corrosion rate and the permeation current densities maintained stable values between 100 hours and after 600 to 700 hours exposure. In NACE A solution, however, after a plateau between 100 hours and 350 hours, a significant decrease of both the corrosion rate and hydrogen permeation down to very low values was measured. This difference is suspected to be due to the formation of a considerably more protective film at the X65 steel entry surface exposed to NACE A solution, compared to pure iron exposed to 35 g/L NaCl.

ACKNOWLEDGEMENTS

REFERENCES

1. "NACE TM0284-2016: Evaluation of pipeline and pressure vessel steels for resistance to hydrogen-induced cracking," NACE International, 2016.
2. "NACE TM0177-2016: Laboratory testing of metals for resistance to sulfide stress cracking and stress corrosion cracking in H2S environments," NACE International, 2016.
3. Y. Song, A. Palencsar, G. Svenningsen, J. Kvarekval, T. Hemmingsen, Corrosion 68, 7 (2012): p. 662–671.
4. J.L. Crolet, M. Pourbaix, A. Pourbaix, "The role of trace amounts of oxygen on the corrosivity of H2S media," Corrosion/91, Paper 22, 10-15 March (1991).
5. H.S. Kuo, H. Chang, W.T. Tsai, Corrosion Science 41, 4 (1999): p. 669–684.
6. A. Kawashima, K. Hashimoto, S. Shimodaira, Corrosion 32, 8 (1976): p. 321–331.
7. T. Zakroczymski, Z.Szklarska-Smiatowska, M.Smiatowski, Werkstoffe und Korrosion 27 (1976).
8. B. Le Boucher, Revue de l'Institut Francais du Petrole 23, 4 (1963): p. 1–66.
9. M.H. Abd Elhamid, B.G. Ateya, K.G. Weil, H.W. Pickering, Corrosion 57, 5 (2001): p. 428–432.
10. M. Kappes, G.S. Frankel, N. Sridhar, R.M. Carranza, J. Electrochem. Soc. 159, C195-C204 (2012).
11. M.D. Deffo Ayagou, C. Mendibide, C. Duret-Thual, J. Kittel, K. Belkhadiri, T.T. Mai Tran, E. Sutter, B. Tribollet, N. Ferrando, Corrosion, accepted (2018).
12. M.D. Deffo Ayagou, T.T. Mai Tran, B. Tribollet, J. Kittel, E. Sutter, N. Ferrando, C. Mendibide, C. Duret-Thual, Electrochim. Acta 282, 775-783 (2018).
13. M.A.V Devanathan and Z. Stachurski, J. Electrochem. Soc. 111, 619-623 (1962).
14. Y. Song, A. Palencsár, G. Svenningsen, J. Kvarekvål, T. Hemmingsen., Corrosion 68, 662-671 (2012).
15. J.L. Crolet, M. Pourbaix, A. Pourbaix, "The Role of trace amounts of oxygen on the corrosivity of H2S media," Corrosion/91 paper 22, 10-15 March, Cincinnati, OH (USA), NACE International (1991).
16. L. Choudhary, D.D. Macdonald, A. Alfantazi, Corrosion 71, 1147-1168 (2015).
17. M.D. Deffo Ayagou, T.T. Mai Tran, B. Tribollet, J. Kittel, E. Sutter, N. Ferrando, C. Mendibide, C. Duret-Thual, Electrochim. Acta 282, 775-783 (2018).
18. M.D. Deffo Ayagou, C. Mendibide, C. Duret-Thual, J. Kittel, K. Belkhadiri, T.T. Mai Tran, E. Sutter, B. Tribollet, N. Ferrando, Corrosion, accepted (2018).
19. S.Wach, A.P.Miodownik, J.Mackowiak, Corrosion Science 6, 271-285 (1966).
20. T. Tran, B. Brown, S. Nesic, B. Tribollet, Corrosion 70, 223-229 (2014).